

Molecular and Cellular Pathobiology

# Selective *In Vivo* Imaging of Syngeneic, Spontaneous, and Xenograft Tumors Using a Novel Tumor Cell–Specific Hsp70 Peptide-Based Probe

Stefan Stangl<sup>1</sup>, Julia Varga<sup>2</sup>, Bianca Freysoldt<sup>1</sup>, Marija Trajkovic-Arsic<sup>3</sup>, Jens T. Siveke<sup>3</sup>, Florian R. Greten<sup>2</sup>, Vasilis Ntziachristos<sup>4</sup>, and Gabriele Multhoff<sup>1</sup>

#### **Abstract**

Although in vivo targeting of tumors using fluorescently labeled probes has greatly gained in importance over the last few years, most of the clinically applied reagents lack tumor cell specificity. Our novel tumor cell-penetrating peptide-based probe (TPP) recognizes an epitope of Hsp70 that is exclusively present on the cell surface of a broad variety of human and mouse tumors and metastases, but not on normal tissues. Because of the rapid turnover rate of membrane Hsp70, fluorescently labeled TPP is continuously internalized into syngeneic, spontaneous, chemically/genetically induced and xenograft tumors following intravenous administration, thereby enabling site-specific labeling of primary tumors and metastases. In contrast with the commercially available nonpeptide small molecule  $\alpha_v \beta_3$ -integrin antagonist IntegriSense, TPP exhibits a significantly higher tumor-to-background contrast and stronger tumor-specific signal intensity in all tested tumor models. Moreover, in contrast with IntegriSense, TPP reliably differentiates between tumor cells and cells of the tumor microenvironment, such as tumor-associated macrophages and fibroblasts, which were found to be membrane-Hsp70 negative. Therefore, TPP provides a useful tool for multimodal imaging of tumors and metastases that might help to improve our understanding of tumorigenesis and allow the establishment of improved diagnostic procedures and more accurate therapeutic monitoring. TPP might also be a promising platform for tumor-specific drug delivery and other Hsp70-based targeted therapies, Cancer Res; 74(23); 6903-12. ©2014 AACR.

#### Introduction

Tumor targeting peptides represent a promising new class of prognostic tools due to their advantageous biodistribution with fast body clearance and their capacity to effectively penetrate viable cells (1–3). However, it is essential that such probes exhibit specific binding to tumor cells and exclude normal tissue. The identification of tumor-selective probes is therefore essential.

In addition to its physiologic, stress-induced appearance in the cytoplasm, HSP70 (Hsp70-1, HspA1A, #3303) has been found to be selectively localized on the plasma

<sup>1</sup>Department of Radiation Oncology, Klinikum rechts der Isar, TU München and CCG - "Innate Immunity in Tumor Biology", Helmholtz Zentrum München (HMGU), Munich, Germany. <sup>2</sup>Institute for Tumor Biology and Experimental Therapy, Georg-Speyer-Haus, Frankfurt/Main, Germany. <sup>3</sup>Department of Medicine II, Klinikum rechts der Isar, TU München, Munich, Germany. <sup>4</sup>Institute of Biological and Medical Imaging, Helmholtz Zentrum München (HMGU), Munich, Germany.

**Note:** Supplementary data for this article are available at Cancer Research Online (http://cancerres.aacrjournals.org/).

Corresponding Author: Gabriele Multhoff, Department of Radiation Oncology, Klinikum rechts der Isar, TU München, Ismaningerstrasse 22, 81675 München, Germany. Phone: 49-89-4140-4514; Fax: 49-89-4140-4299; E-mail: gabriele.multhoff@lrz.tu-muenchen.de

doi: 10.1158/0008-5472.CAN-14-0413

©2014 American Association for Cancer Research.

membrane of a broad variety of different murine and human tumors. Because of its absence in the membranes of normal cells, targeting membrane Hsp70 on tumors offers unique opportunities for the detection, screening, and staging of diseases (4–7), as well as for drug development and treatment evaluation of a wide variety of neoplasms in future theranostic approaches (8–10).

Screening of tumor biopsies and their corresponding normal tissues of well over 1,000 patients has shown that the majority of the primarily diagnosed carcinoma samples, but none of the tested corresponding normal tissues, exhibited an Hsp70-membrane-positive phenotype (5). Furthermore, we have previously shown that Hsp70-membrane positivity is increased in stressed tumor cells that also exhibit elevated cytosolic Hsp70 levels. In the cytosol, Hsp70 acts in an antiapoptotic manner and enhances survival of the tumor cells following therapies such as chemo- and radiotherapy (11). Most importantly, an Hsp70-membrane-positive tumor phenotype has been shown to be associated with a significantly decreased overall survival in cancerous diseases such as leukemia (12), lung, breast (13), lower rectal carcinomas (14), prostate (8), and liver cancer (15). These findings demonstrate that Hsp70 positivity might serve as a useful marker for prediction of clinical outcome. The potential therapeutic value of membrane Hsp70 has been demonstrated in a previous study that reported on the generation of an Hsp70-specific antibody termed cmHsp70.1 to specifically induce antibody-dependent cellular cytotoxicity of tumor cells *in vitro* and *in vivo* (16, 17).

Herein, we describe a novel peptide-based probe that binds to membrane Hsp70. Because of its remarkable tumor specificity and capacity for internalization (18), this probe has been termed Hsp70 tumor cell-penetrating peptide (TPP). TPP, which comprises the amino acid sequence aa<sub>450-463</sub> (TKDNNLLGRFELSG) of the C-terminal oligomerization domain of Hsp70, binds to tumor cells with high affinity in vivo as well as in vitro. The specificity of TPP toward Hsp70 was shown by ELISA (Supplementary Fig. S1). As recently shown by Mahalka and colleagues (19), the C-terminal and N-terminal domain of Hsp70 are exposed to the extracellular milieu of tumor cells if presented on the plasma membrane. Although in vitro TPP exhibits similar binding characteristics toward Hsp70 than the cmHsp70.1 monoclonal antibody (16, 17), TPP exerts a better biodistribution, in vivo.

#### **Materials and Methods**

#### Animals

BALB/c, FvB, and SHO-*Prkdc*<sup>scid</sup>*Hr*<sup>Hr</sup> (SHO) mice were obtained from an animal breeding colony (Charles River and Harlan Winkelmann) and were maintained in pathogen-free, individually ventilated cages (Tecniplast). All animal experiments were approved by the District Government of Upper Bavaria and performed in accordance with the German Animal Welfare and Ethical Guidelines of the Klinikum rechts der Isar, TUM, Munich, Germany. Tumors were examined after the animals were sacrificed by cervical dislocation.

#### Syngeneic tumor models

CT26 mouse colon adenocarcinoma cells ( $5 \times 10^5$ ) or 4T1 mammary carcinoma cells ( $2.5 \times 10^5$ ; ATCC, authentication not applicable for mouse cell lines) were harvested in the exponential growth phase and injected subcutaneously in the neck or orthotopically into the mammary fad pad of 8-weekold, female BALB/c mice, respectively. Primary tumor growth was followed by ultrasonic measurements (Logiq-5, GE Healthcare). Intraoperative *in vivo* imaging was performed post mortem on exposed tumors when the CT26 tumors reached a size of approximately 0.4 cm $^3$ . 4T1-derived tumors and lung metastases were investigated after 25 to 30 days of tumor growth.

#### Xenograft tumor models

To test the capacity of TPP to recognize human tumors,  $5\times10^6$  cells from the following human carcinoma cell lines were implanted subcutaneously into the neck area or orthotopically into the mammary fat pad of 8- to 10-week-old, female SHO mice: colon carcinoma cell lines HCT-116 (ATCC) and CX-2 (DKFZ), mammary carcinoma cell lines MCF-7, MDA-MB231 and T-47D (ATCC), pancreas carcinoma cell lines Panc-1, MIA PaCa-2 (provided by J.T. Siveke) and COLO357 (Leibniz-Institute DSMZ, Braunschweig,

Germany), small-cell lung cancer H1339, non-small cell lung cancer (NSCLC) A549 (n.t.), head and neck carcinoma FaDu (all ATCC) and Cal-33 (Leibniz-Institute DSMZ), as well as the human cervix carcinoma HeLa (ATCC). Mice were sacrificed and intraoperative *in vivo* imaging was performed on the exposed tumors when tumors had reached a volume of 0.2 to 0.4 cm<sup>3</sup>. If not stated otherwise, cell line authentication was performed by short tandem repeat profiles that are generated by simultaneous amplification of multiple short tandem repeat loci by ATCC and DSMZ. Cells were not cultured for longer than 5 months after testing.

#### Colitis-associated spontaneous tumor model

Spontaneous colonic tumors were induced in 8-week-old female FvB mice (Charles River) using an established approach. Briefly, mice were injected intraperitoneally with a single dose of azoxymethane (AOM; Sigma-Aldrich) at 10 mg/kg body weight. Following AOM treatment, the mice were subjected to three cycles of dextran sulfate sodium salt (MP Biomedicals) administration in their drinking water (20). After 15 to 18 weeks of tumor development, the mice were sacrificed and the colon was resected for experiments. The presence of colorectal tumors was confirmed using standard histologic techniques.

### **Endogenous pancreatic ductal adenocarcinoma mouse** model

The spontaneous pancreatic ductal adenocarcinoma (PDAC) mouse model ( $Ptf1a^{+/Cre}$ ; $Kras^{+/LSL-G12D}$ ; $p53^{LoxP/LoxP}$ , CKP) has been described previously (21). After sacrificing, the abdominal cavity of tumor-bearing mice, including the pancreas, was exposed for  $in\ vivo$  imaging of the tumor area and surrounding normal tissue.

#### **Toxicity testing**

Potential toxic effects of TPP were investigated by injecting healthy BALB/c mice intravenously with 500 and 1050  $\mu g$  of TPP. Concentrations up to 500  $\mu g$  of TPP per mouse were tested in tumor-bearing mice (s.c. tumors, size 0.4  $cm^3$ ). The health status and the general behavior of mice were inspected. Animals were sacrificed on day 5 and the heart, liver, spleen, lung, and kidneys examined for pathologic changes using standard histologic techniques.

#### Flow cytometry

The membrane-Hsp70 phenotype of tumors grown *in vivo* was determined by flow-cytometric analysis of single cell suspensions that were generated following 30 minutes collagenase/dispase digestion using FITC-conjugated cmHsp70.1 mAb (IgG1, multimmune GmbH) or carboxyfluorescein-conjugated TPP (TPP[CF]). Cell suspensions were incubated with the appropriate reagent for 30 minutes at  $4^{\circ}\mathrm{C}$ , after which they were washed and viable (7-AAD negative) cells were analyzed using a FACSCalibur flow cytometer (Becton Dickinson). Gating was applied to distinguish the CD45 $^-/\mathrm{CD140b}^-$  tumor cell population from CD45 $^-/\mathrm{CD140b}^+$  fibroblasts and CD45 $^+/\mathrm{F4/80}^+$  macrophages.

### TPP, control peptide, and IntegriSense 750 in imaging procedures

In in vivo imaging experiments, Cv5.5 or DvLight750-conjugated Hsp70-specific 14-mer TPP (OEM manufactured by Thermo Fischer) was compared with the unspecific scrambled control peptide (CP, OEM manufactured by Thermo Fischer) and with IntegriSense 750 (IS750, PerkinElmer; Supplementary Fig. S2). The intraoperative imaging procedure, which captured color and fluorescence images of the exposed tumors and its surrounding normal tissue, was configured to simulate an intraoperative imaging situation. TPP[Cy5.5] or CP[DL750] (100 µg, equal to 45 nmol per animal) or IS750, at the recommended dose of 2 nmol per animal, was injected into the tail vein of tumor-bearing mice. Concentrations above 2 nmol resulted in a higher staining of healthy tissues and thus negatively affected the tumor-to-background ratio (TBR; data not shown). Signal specificity was determined by calculating the ratio of the mean signal intensity in the exposed tumor tissue and that of the surrounding normal tissue (TBR; ref. 22). Kinetic studies were performed 12, 24, 48, and 72 hours after tail vein bolus injection of TPP[Cy5.5] and CP[DL750]. All other experiments were performed 24 hours after intravenous injection of the respective probes.

Fluorescent images were acquired by illuminating the specimens using 670 and 740 nm diode lasers and guiding the emitted fluorescence through appropriate emission filters before capturing it using a back illuminated EM-CCD camera (iXon DU888, Andor), as described previously (16). A more detailed description of the imaging procedures is shown in the Supplementary Section.

#### **Biodistribution studies**

For biodistribution, tumor-bearing mice were sacrificed 12, 24, or 48 hours after intravenous injection of TPP[Cy5.5]. Fluorescent signal intensities of 0.25 cm³ tissue cubes, taken from the tumor, spleen, pancreas, liver, lung, duodenum, kidney, heart, and 0.25 mL of peripheral blood were measured as described above. Agarose-gel cubes with standardized concentrations were used to calculate the probe concentrations in the investigated tissue samples. Detailed information concerning the quantification of TPP[Cy5.5] is provided in Supplementary Fig. S6.

#### Histology, IHC, and fluorescence microscopy

Paraformaldehyde-fixed and paraffin-embedded tissue sections (2  $\mu m)$  were stained with hematoxylin and eosin using standard procedures. For IHC on cryosections, unspecific mouse-on-mouse reactions were blocked using a M.O.M. kit (Vector Labs) and stained with cmHsp70.1 mAb following antigen retrieval in citrate buffer. The quantification and volumetric analysis of lung metastases were performed using consecutive tissue sections (100  $\mu m$ ) using Aperio ImageScope software (Leica).

For microscopic *in situ* fluorescence analysis, TPP[CF] (100  $\mu$ g) and the recommended dose of IntegriSense 750 (IS[750]) were injected intravenously into tumor-bearing mice and allowed to circulate for 24 hours. Tissue was collected and 8  $\mu$ m cryosections counterstained with DAPI (DAKO) and

examined microscopically using a Zeiss Observer Z1 (Carl Zeiss) equipped with standard filters for GFP and Cy7 after 4 minutes of fixation with 1.8% w/v PFA.

#### Statistical analysis

Statistical analysis was performed using the Student t test. Data are mean  $\pm$  SD. P values  $\leq$  0.05 were considered as being significant different between the compared groups.

#### Results

## The membrane-bound form of Hsp70, but not $\beta$ 3-integrin, is present on a wide variety of human and murine tumors

To examine the presence of the investigated reporter epitopes on cells in vivo, a broad variety of murine and human tumors were screened for the presence of membrane Hsp70 and  $\beta 3$ -integrin (CD61), the target epitopes for TPP and Integri-Sense, respectively. This screening included colon, mammary, pancreatic, lung, head and neck, and cervical carcinomas derived from syngeneic, chemically induced, spontaneous and xenograft mouse models. Flow-cytometric analysis of viable cells derived from the solid tumors demonstrated that all of the cells examined exhibited a comparable membrane Hsp70 staining pattern using the cmHsp70.1 monoclonal antibody or the TPP probe (Fig. 1; Table 1). This finding further emphasizes the fact that targeting membrane Hsp70 could serve as a universal approach for diagnosing a wide variety of tumor entities.

For flow-cytometric analysis, a cell population was defined to be membrane positive if as more than 20% of the cells were stained. The threshold of 20% was defined upon screening of a large panel of healthy human tissues, including human peripheral blood lymphocytes, fibroblast, and healthy tissues surrounding tumor (n = 86). CD61 staining revealed  $\alpha_v \beta_3$ -integrin positivity on mouse colon (CT26) and mammary (4T1) carcinoma, on human mammary (MDA-MB231, T-47D) and head and neck (CAL-33) carcinoma, as well as on human and mouse pancreatic carcinoma (PDAC, Panc-1, MIA PaCa-2, COLO357). However, no β<sub>3</sub>-integrin expression could be detected on human colon (HCT-116, CX-2), mammary (MCF-7), lung (H-1339), or cervical (HeLa) carcinoma cells. Cells derived from a murine colitis-associated carcinoma (CAC) model showed a heterogeneous CD61 expression. These data indicate that, in comparison with  $\beta_3$ -integrin, Hsp70 is more frequently expressed on human and murine tumors. However, tumor cell specificity is critical for targeting strategies. Therefore, the presence of membrane Hsp70 and β3-integrin on tumor-residing CD45<sup>+</sup>/F4/80<sup>+</sup> macrophages and CD45<sup>-</sup>/CD140b<sup>+</sup> fibroblasts was investigated. TPP only weakly stains (below 10%) tumor-associated fibroblasts and tumor-infiltrating macrophages; in contrast, β3-integrin positivity was found on more than 60% of tumor-associated fibroblasts and tumor-infiltrating macrophages (Fig. 1B). To test Hsp70 positivity on tumors, cryosections were stained with the Hsp70-specific antibody cmHsp70.1. Although tumor cells of the various tumor models were positive, cells of the tumor microenvironment remained negative for Hsp70. A representative staining of a PDAC tumor is shown in Supplementary Fig. S3.

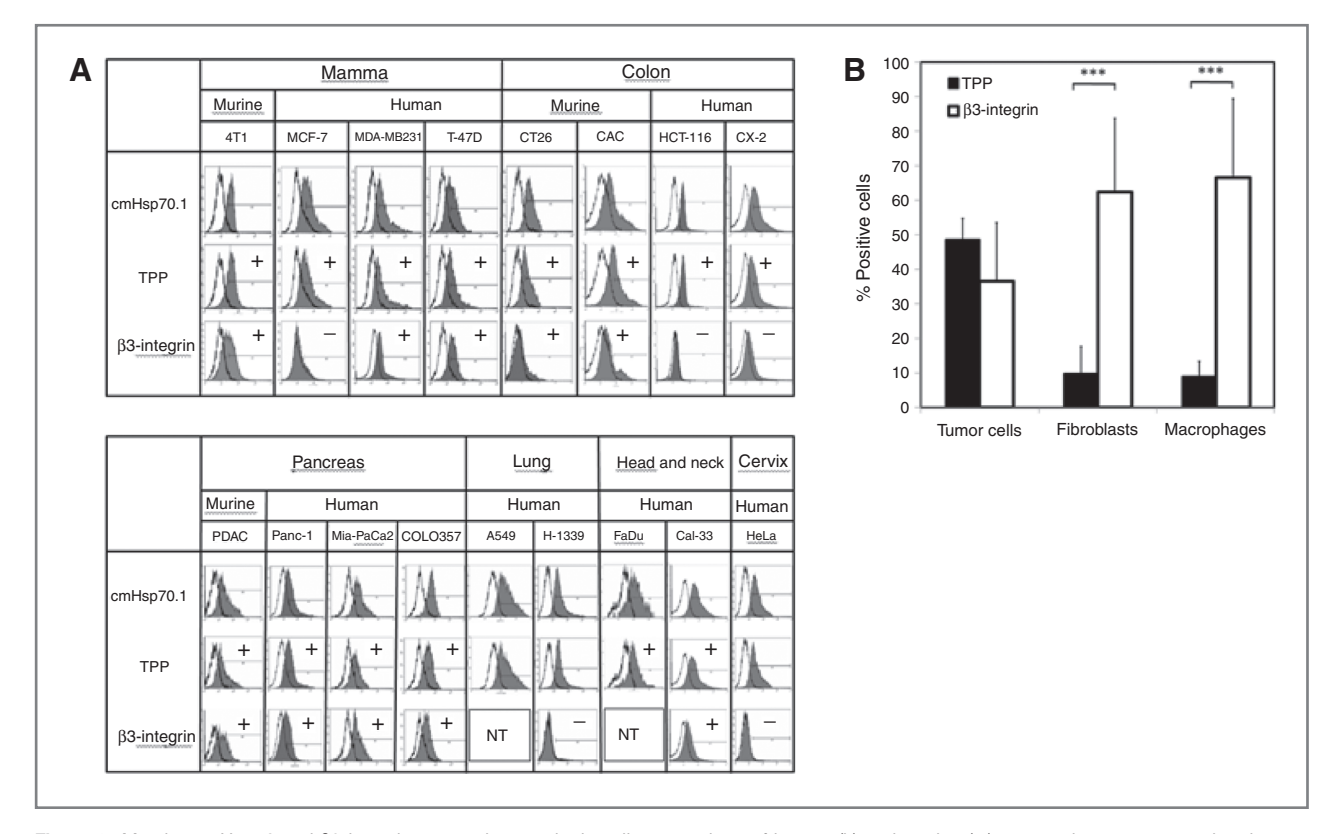


Figure 1. Membrane-Hsp70 and β3-integrin expression on single cell suspensions of human (h) and murine (m) tumors that were grown in mice. A, comparison of the binding capacity of cmHsp70.1 full-length antibody (top), TPP (middle), and β3-integrin antibody (bottom) to mammary (m4T1, hMCF-7, hMDA-MB231, hT-47D), colon (mCT26, mCAC, hHCT-116, hCX-2), pancreas (mPDAC, hPanc-1, hMiaPaCa2, hCoL0357), lung (hA549, hH-1339), head and neck (hFaDu, hCal-33), and cervix (hHeLa) carcinomas. Results are expressed as log fluorescence intensity versus relative cell numbers. The IgG1 isotype-matched control is indicated in white and membrane staining in gray histograms. B, membrane positivity of TPP (black bars) and β3-integrin (white bars) on cells of the tumor microenvironment in comparison with β3-integrin-positive tumors. Membrane staining of TPP remained significantly lower in macrophages ( $P = 1.54 \times 10^{-7}$ ) and fibroblasts ( $P = 4.67 \times 10^{-8}$ ), compared with β3-integrin. Averaged tumor cell positivity revealed no significant difference between TPP and β3-integrin staining.

#### TPP is not toxic in vivo

To examine potential toxic side effects of TPP, healthy and tumor-bearing BALB/c mice were injected intravenously with 500 to 1,050  $\mu g$  of TPP, which is equivalent to 25 to 50  $\mu g/g$  of their body weight. Gross monitoring of the mice did not show any toxic reactions such as skin ulcerations or toxic death at any of the tested doses. Nor did any animal exhibit any loss of weight or change in mobility. Histologic examination of the heart, liver, spleen, lung, and kidney on day 5 after injection by a veterinarian, revealed no pathologic changes. An examination of the effects of TPP concentrations up to 500  $\mu g$  in tumor-bearing mice also did not exert any side effects.

## TPP accumulates within the tumor with maximal specificity 24 hours postintravenous injection

To investigate the *in vivo* circulation and tumor-homing properties of TPP, we analyzed its biodistribution in CT26 tumor-bearing mice. The accumulation of TPP in different organs was determined 12, 24, and 48 hours after intravenous injection of  $100 \,\mu g$  TPP[Cy5.5] by measuring fluorescent signal intensities in the tumor, spleen, pancreas, liver, lung, duodenum, kidney, heart, and in the peripheral blood (Fig. 2).

A strong TPP[Cy5.5] signal could be detected within the tumor  $(7.6\pm0.7~\mu\text{g/cm}^3)$  12 hours after intravenous injection. This reached a maximum after 24 hours  $(10.4\pm2.2~\mu\text{g/cm}^3)$  and dropped after 48 hours. TPP accumulation was significantly lower at all investigated time points in all other tested organs, except the kidney. The concentration of TPP[Cy5.5] reached its maximum in the kidney after 12 hours at 13.7  $\pm$  0.6  $\mu\text{g/cm}^3$ , and this accumulation was followed by a sharp drop, 24 and 48 hours postinjection. These data further confirm the tumor specificity of TPP and indicate that TPP is cleared from the body by renal excretion.

In further experiments, we investigated the optimal time point for *in vivo* imaging in a CT26 tumor model (subcutaneously) 2 weeks after tumor injection (Supplementary Fig. S5A) and a metastasizing 4T1 mammary carcinoma model (orthotopically) 3 to 4 weeks after tumor injection (Supplementary Figs. S5B and S5C and S7). TPP[Cy5.5] yielded maximal TBR in primary tumors 24 hours after injection of the probe, whereas the peak TBR in metastasized lungs occurred after 48 hours. The scrambled control peptide CP[DL750] did not show any specific accumulation in tumor tissue (Supplementary Fig. S5A–S5C).

**Table 1.** Binding of TPP to different membrane-Hsp70–positive colon, mammary, pancreas, lung, head and neck, and cervix mouse and human tumors

	Colon				Mammary				
	Murine		Human		Murine	Human			
%	CT26	CAC	HCT-116	CX-2	4T1	MCF-7	MDA-MB231	T-47D	
Hsp700	$55.5\pm5.5$	$51.2\pm0.8$	$63.3 \pm 9.3$	$56.6 \pm 8.3$	$\textbf{56.3} \pm \textbf{3.5}$	$58.0 \pm 3.6$	$63.3\pm13.3$	$48.0\pm4.2$	
TPP	$42.0 \pm 4.3$	$52.8\pm7.5$	$59.0\pm7.9$	$45.2\pm5.2$	$47.5\pm2.1$	$46.0 \pm 5.6$	$62.5\pm15.6$	$43.5 \pm 2.1$	
CD61	$26.5\pm7.8$	$23.0 \pm 7.1$	$15.3\pm1.5$	$14.0\pm5.0$	$38.3 \pm 3.2$	$13.0\pm1.7$	$20.0\pm5.6$	$55.5\pm2.1$	

		Pan	creas		Lung		Head and neck		Cervix
	Murine	Murine Human			Human		Human		Human
%	PDAC	Panc-1	MIAPaCa-2	COLO357	A549	H-1339	FaDu	Cal-33	HeLa
Hsp70 TPP CD61	$50.0 \pm 8.6 \\ 45.0 \pm 1.4 \\ 50.0 \pm 5.7$	$46.0 \pm 4.2 \\ 47.0 \pm 7.1 \\ 36.0 \pm 2.8$	$58.5 \pm 7.6 \\ 42.0 \pm 6.6 \\ 70.0 \pm 11.3$	$57.8 \pm 9.3$ $49.5 \pm 4.9$ $20.0 \pm 9.9$	$76.3 \pm 1.5 \\ 58.3 \pm 7.6 \\ \text{n.t.}$	$60.0 \pm 7.5 \\ 67.0 \pm 5.7 \\ 4.0 \pm 1.8$	$59.0 \pm 8.5 \\ 53.5 \pm 0.7 \\ \text{n.t.}$	$68.1 \pm 8.5 \\ 52.0 \pm 4.2 \\ 23.5 \pm 3.5$	$55.0 \pm 18.4 \\ 63.0 \pm 4.2 \\ 5.0 \pm 5.6$

NOTE: The proportion of membrane-Hsp70–positive cells was measured with cmHsp70.1 antibody and TPP peptide on single cell suspensions of *in vivo*-grown human and mouse tumors of different entities. The expression of CD61 ( $\beta$ 3-integrin) was also determined on these tumor cells. A sample was determined as membrane positive if more than 20% of the cells showed a positive staining. Abbreviation: n.t., not tested.

## The specific accumulation of TPP in syngeneic primary tumors and metastases is superior to that of IntegriSense

To confirm the specificity of TPP[Cy5.5] for primary tumors and metastases *in vivo*, we simultaneously injected 100 µg of TPP[Cy5.5] and the recommended dose of Integri-Sense 750 (IS[750]) into CT26 and 4T1 tumor-bearing mice,

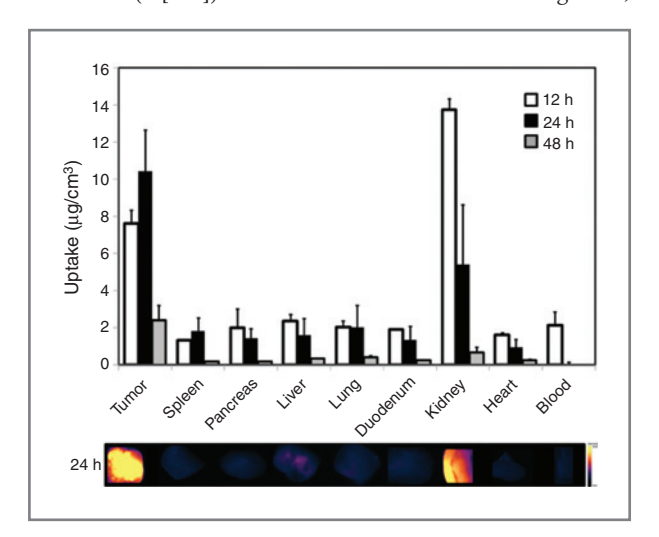


Figure 2. Biodistribution of TPP[Cy5.5] in CT26 tumor-bearing mice, assessed by NIRF quantification. Tumors and organs of CT26 tumor-bearing mice were collected 12, 24, and 48 hours (white, black, and gray bars, respectively) after intravenous injection of TPP[Cy5.5] into the tail vein. The fluorescence signals of the probe were analyzed, ex vivo. Two to three mice per time point were assessed; graph bars show mean values ± SD.

24 hours before in vivo imaging. Although TPP[Cy5.5] and IS[750] both clearly delineate the tumor, IS[750] signals can also be found in normal tissue surrounding the tumor (Fig. 3A and B, true color images of the region of interest is depicted on the left). TPP[Cy5.5] exhibited a significantly higher TBR than IS[750] (P = 0.0004 and 0.003, respectively). To further investigate the specificity of the probes, ex vivo imaging of dissected lungs containing metastases was performed. Quantification of metastases can be found in Supplementary Fig. S4. The TBR for IS[750] imaging was also lower than that for TPP[Cy5.5] (P = 0.04; Fig. 3C, bottom) in distant lesions. Although the delineation of metastases by TPP[Cy5.5] and IS[750] was comparable, the enrichment of IS[750] in normal lung tissue is marginally higher (Fig. 3C, top). The specificity and colocalization of TPP and IS was further confirmed on cryo-sections of the lesions, which were obtained 24 hours after intravenous injection of TPP[CF] and IS[750] (Fig. 3D). Both probes specifically enriched in the primary tumor and lung metastases, however, a background staining of IS[750] remained in healthy lung tissue. These data demonstrate that, although both compounds specifically stain tumors and metastases, TPP is more effectively washed out of normal tissue and therefore provides a better signal-to-background contrast than IntegriSense.

## The specific tumor-homing capacity of TPP is higher than that of IntegriSense in endogenous tumor models

To more realistically mimic the histologic and molecular features of human tumors in *in vivo* imaging, we took advantage of chemically induced and endogenous mouse models of colorectal (CAC) and pancreatic (PDAC) cancer. Flow-

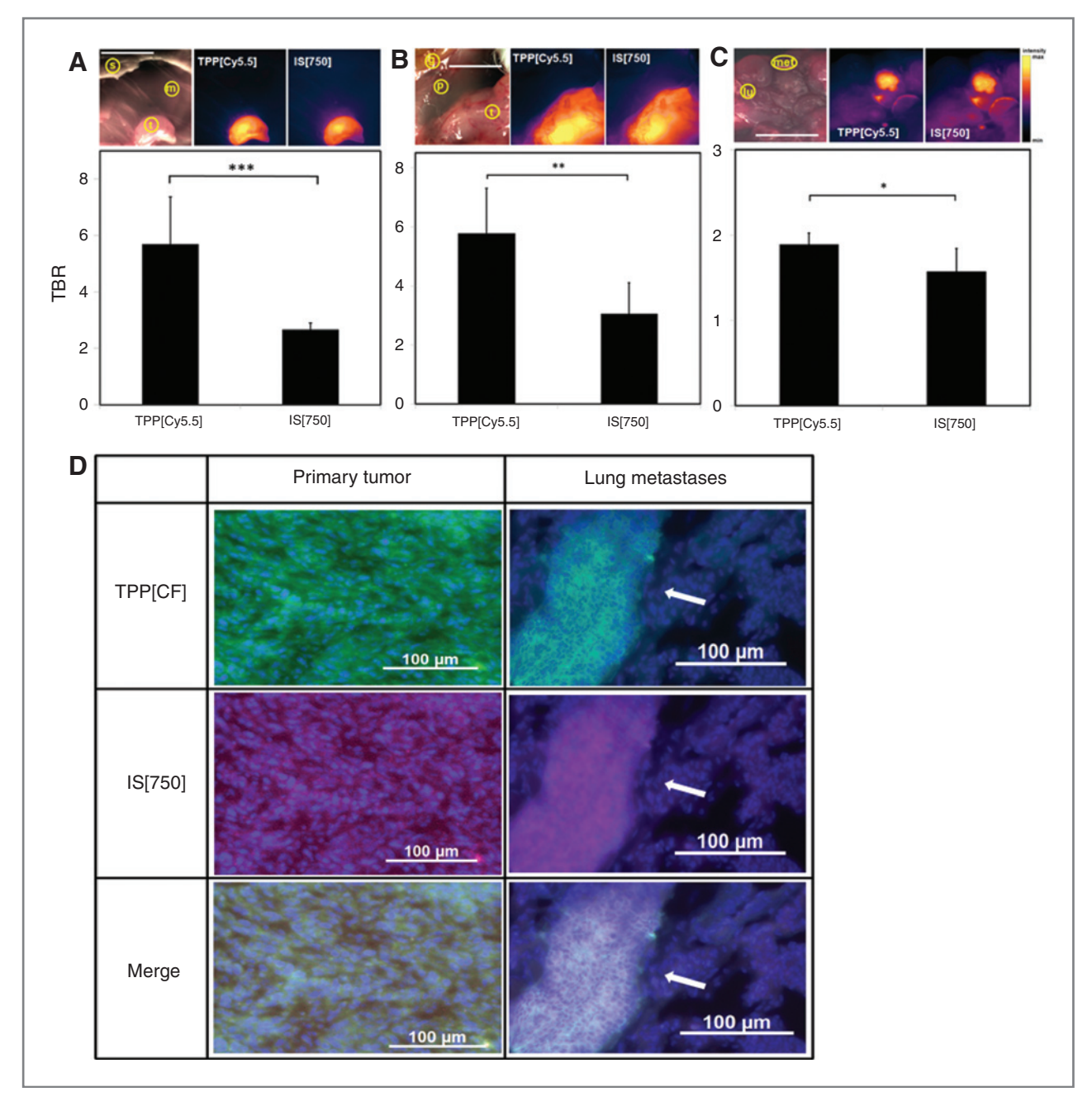


Figure 3. Intraoperative *in vivo* imaging and fluorescence microscopy of syngeneic tumor models after the injection of TPP[Cy5.5] and IS[750]. A, NIRF imaging of CT26 tumors that were injected subcutaneously into the neck area, B and C, 4T1 tumors injected orthotopically (B) and lung metastases (C) derived thereof. Top, true color images of tumor (t) and metastases (met), as well as surrounding normal tissue, including muscle (m), skin (s), gut (g), peritoneum (p), and lung (lu; left, scale bars, 5 mm). Corresponding pseudocolor fluorescence images were taken 24 hours after intravenous injection of TPP[Cy5.5] (middle) and IS[750] (right) into the same animal. Bottom, TBR, 24 hours after intravenous injection of TPP[Cy5.5] and IS[750]. The data are shown as mean  $\pm$  SD [n=4 (CT26) and 6 (4T1)]; \*, P<0.05; \*\*, P<0.01; \*\*\*, P<0.001. D, fluorescence microscopy of primary tumor (left) and lung tissue, including metastases, indicated by arrows (right), 24 hours after intravenous injection of TPP[CF] (top) and IS[750] (middle) in the same animal. Bottom, an overlay of both compounds. Scale bars, 100  $\mu$ m.

cytometric analysis of isolated tumor cells revealed Hsp70 and  $\beta$ 3-integrin positivity in both models (Table 1). To investigate the *in vivo* tumor targeting properties in these models, NIR imaging of tumors was performed 24 hours after intravenous injection of TPP[Cy5.5], CP[DL750], and IS[750] (Fig. 4).

Although the fluorescence signals of both TPP[Cy5.5] and IS[750] clearly delineated the exposed colon and pancreatic tumors, a clear background staining in the tumor-surrounding normal colon tissue was observed following administration of IS[750]. In the colitis-induced tumors, the TBR of TPP[Cy5.5]

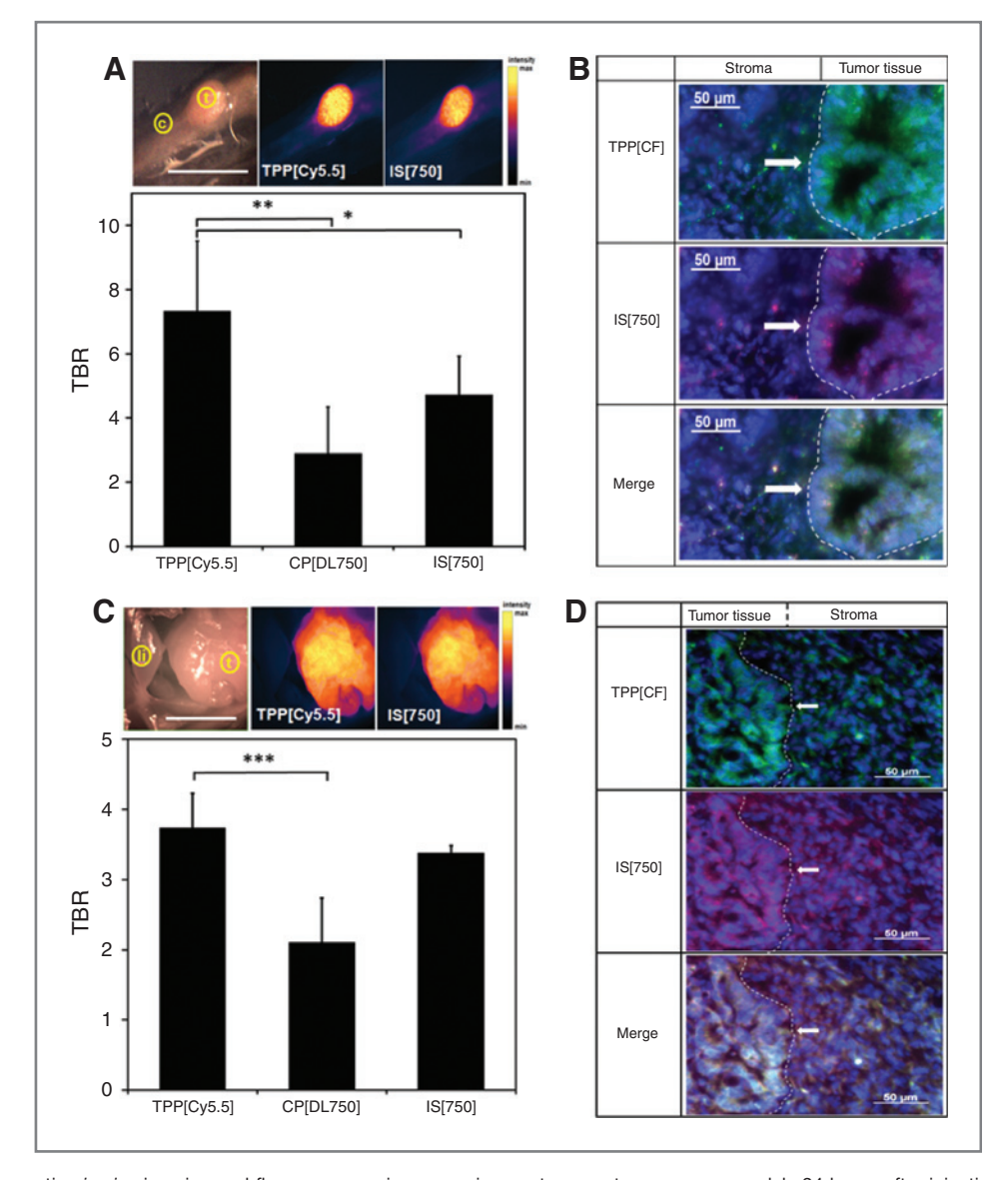


Figure 4. Intraoperative *in vivo* imaging and fluorescence microscopy in spontaneous tumor mouse models 24 hours after injection of TPP[Cy5.5], CP[DL750], and IS[750]. A, NIRF imaging of CAC. Top, true color image of tumor (t) and surrounding colon tissue (c; scale bar, 5 mm), with corresponding pseudocolor fluorescence images 24 hours after intravenous injection of TPP[Cy5.5] (middle) and IS[750] (right). Bottom, TBR, 24 hours after intravenous injection of TPP[Cy5.5], CP[DL750], and IS[750]. The data are shown as mean  $\pm$  SD, n=5 (TPP[Cy5.5]), 4 (CP[DL750]), and 3 (IS[750]). \*, P < 0.05; \*\*, P < 0.05; \*\*, P < 0.01. B, fluorescence microscopy of identical cryosections of a representative primary tumor (left) and normal tissue (right) 24 hours after intravenous injection of TPP[CF] (top) and IS[750] (middle) into the same animal. Bottom, an overlay of both compounds with enhanced enrichment of TPP[CF] in crypt-like neoplastic tissue (arrows), compared with IS[750]. Normal tissue remained negative for both compounds. Scale bars, 50  $\mu$ m. C, NIRF imaging of PDAC. Top, true color image of tumor (t) and surrounding normal tissue, including liver (li; left, scale bar, 5 mm), and corresponding pseudocolor fluorescence images, 24 hours after intravenous injection of TPP[Cy5.5] (middle) and IS[750] (right). Bottom, TBR 24 hours after intravenous injection of the compounds. The data are shown as mean  $\pm$  SD of n=7 (TPP[Cy5.5]), 6 (CP[DL750]), and 2 (IS[750]) animals. \*\*\*\*, P < 0.001. D, fluorescence microscopy of identical cryosections of primary tumor tissue (left) including fibrosis of the tumor microenvironment (right) 24 hours after intravenous injection of TPP[CF] (top) and IS[750] (middle). Bottom, an overlay with a comparable enrichment of both compounds in carcinoma tissue and additional IS[750] staining of cells of the tumor microenvironment. Scale bar, 50  $\mu$ m.

was significantly higher than that of CP[DL750] (P = 0.005) and IS[750] (P = 0.016; Fig. 4A). The cellular distribution of the compounds at a microscopic level was analyzed using cryosections of the resected tumors that were obtained 24 hours after intravenous injection of TPP[CF] and IS[750]. Although a strong cytosolic signal of TPP[CF] in predominantly crypt-like

tumor structures (white arrows) was observed, IS[750] treatment resulted in a weaker and more heterogeneous staining pattern (Fig. 4B). Our recent demonstration that membrane Hsp70 is rapidly endocytosed in tumor cells under physiologic conditions (18) provides an explanation for the cytosolic staining pattern of tumors.

The uptake capacities of TPP and IntegriSense were also investigated using an endogenous pancreatic PDAC model, which has an activating mutation in the Kras oncogene concomitant with a deletion of the tumor suppressor Tp53 (21). Tumor cells of this model exhibited strong membrane positivity of both Hsp70 and \( \beta \)-integrin (Table 1). Imaging of the pancreatic tumors was performed after opening of the peritoneal cavity; the stomach, liver, and gut were used to calculate the background fluorescence. The TBR for TPP[Cy5.5] was significantly higher than that of the control peptide (P = 0.0001) and comparable with that of the integrin  $\alpha_v \beta_3$ -targeting compound IS[750] (Fig. 4C). Figure 4D shows fluorescence images of a cryo-sliced pancreatic tumors 24 hours after simultaneous injection of TPP[CF] and IS[750]. Although both compounds stained tumor cells equally (left, white arrows), cells of the tumor microenvironment showed a weaker staining with TPP[CF] (right).

## TPP has a higher capacity to specifically target human xenograft tumors than IntegriSense

To confirm the tumor homing capacities of TPP[Cy5.5] in human tumors, imaging experiments were performed in 13 different human tumor cell lines derived from six entities (colon, mammary, pancreas, head and neck, cervix, and lung; Fig. 5). The TBRs for TPP[Cy5.5] in the xenograft tumors ranged from 5.6  $\pm$  1.6 (mammary carcinoma cell line, MDA-MB231) to 7.8  $\pm$  1.4 (squamous cell carcinoma cell line of the head and neck, Cal-33), all of which were significantly higher than those of CP[DL750]. This indicates a specific enrichment of TPP[Cy5.5] in all of the investigated xenograft tumors. Because it is known that the majority of human pancreatic carcinomas are positive for  $\beta_3$ -integrin (22), we included three pancreas tumor xenograft models

(Panc-1, MiaPaCa-2, COLO357) in our experiment. These models revealed substantial Hsp70 and  $\beta_3$ -integrin positivity (Table 1; Fig. 1). Although IS[750] produced higher TBRs in the pancreatic tumors compared with the other xenograft models that were examined, TPP[Cy5.5] yielded significantly higher ratios in two of these three models [P=0.04 (Panc-1) and P=0.03 (COLO357)].

Other human carcinoma cell lines that were determined as being  $\beta 3$ -integrin positive were T-47D, MDA-MB-231 (mammary carcinomas), and Cal-33 (squamous cell carcinoma of the head and neck; see Table 1). The TBRs of IS[750] fluorescence of T-47D and Cal-33 also were significantly lower than the TBRs for TPP[Cy5.5] (P=0.04 and 0.02, respectively). The TBR for IS[750] in all  $\beta 3$ -integrin negative tumors remained clearly below the TBRs for TPP[750]. These data indicate that TPP might be a powerful tumor targeting agent for the detection, diagnosis, and targeting of several entities in humans.

#### **Discussion**

Interest in the use of peptides as innovative cancer diagnostic and tumor-specific drug delivery tools has increased (1–3). However, one of the most critical issues in cancer detection using tumor-targeting probes is specificity, as most of the recently used markers also bind to tumor-associated stroma and other cells. Despite many reports on tumor markers in oncology, the number of clinically useful, tumor-specific markers with prognostic relevance remains low (23–26). It was shown that membrane Hsp70 is present on nearly all aggressive tumor cells from a wide variety of murine and human tumor entities (4–8, 11–15). Therefore, membrane Hsp70 is of prognostic value and fulfills the criteria for an effective tumor targeting molecule.

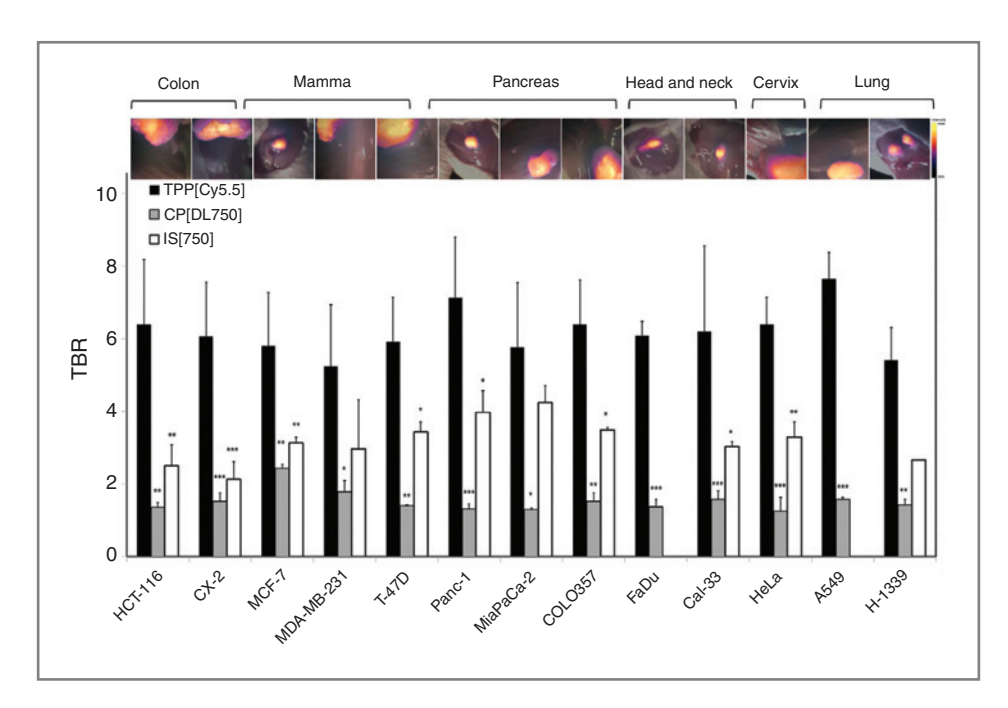


Figure 5. Intraoperative in vivo imaging of xenograft tumors 24 hours after intravenous injection of TPP[Cy5.5], CP[DL750], and IS[750]. Top, overlay of intraoperative true color and fluorescence pseudocolor images of subcutaneous tumors and the surrounding normal tissue 24 hours after intravenous injection of TPP[Cy5.5]. Bottom, TBR, 24 hours after intravenous injection of TPP[Cv5.5] (black bars), CP[DL750] (gray bars), and IS[750] (white bars). The data are shown as mean  $\pm$  SD of two to five mice (H-1339, IS[750]); significance was calculated in comparison with TPP[Cy5.5]; \*, P < 0.05; \*\*, P < 0.01; \*\*\*. P < 0.001.

Given the widespread expression of membrane Hsp70 in different tumor entities and its prognostic relevance, this study evaluated TPP as a tumor homing peptide probe in a wide range of murine and human tumor models. TPP was shown to be highly specific (18) and is therefore an extremely useful tool for *in vivo* tumor detection and diagnosis. Targeting membrane Hsp70 with TPP is advantageous due to its rapid intracellular uptake, biodistribution, and tumor cell–selective accumulation. Similar to Hsp70, an ectopic and tumor-selective expression of Hsp90 has been utilized for the internalization of optical and radioiodinated tethered Hsp90 inhibitors (27).

The use of a colitis-associated colon carcinoma (20) and an endogenous pancreatic tumor model (21) allowed ample mimicking of the human situation in terms of tumor morphology and microenvironment, whereas the xenograft models of colon, mammary, pancreas, lung, head and neck, and cervix carcinoma were used to screen the performance of TPP in numerous human-derived malignant tumors in vivo. TPP was able to specifically detect and penetrate each of the tested tumors at high yields, in vivo (Figs. 3-5; Supplementary Fig. S7A and S7B). Furthermore, TPP specifically stains single cell suspensions of solid tumors, in vitro (Fig. 1A; Table 1). We also compared the in vitro and in vivo binding specificity of TPP with the neoplastic cells of various tumor models and nontransformed cells of the tumor stroma with that of a scrambled control peptide and the commercially available marker IntegriSense, which has been shown to stain different tumor entities, including pancreatic cancers, in vivo (28-31). The TBRs for TPP were higher than that of a control peptide and IntegriSense for all of the investigated tumors.

Flow-cytometric analysis revealed that the ligand of IntegriSense,  $\beta_3$ -integrin, was absent in five of the 11 human tumor xenografts, whereas all tested human and murine tumors were found to be highly membrane-Hsp70 positive (Fig. 1A; Table 1).

To reflect the more complex *in vivo* situation, we broadened our investigations to non-neoplastic cells of the tumor stroma. We used flow cytometry to analyze the presence of membrane Hsp70 and  $\beta_3$ -integrin on macrophages and fibroblasts in single cell suspensions derived from solid tumors. Both cell types show a low background fluorescence of membrane-Hsp70 but high  $\beta_3$ -integrin positivity (Fig. 1B). Although macrophages internalize IntegriSense and TPP *in vivo*, only a minimal level of TPP staining was detected in tumor-associated fibroblasts. Other studies demonstrated the presence of integrins, including  $\beta_3$ -integrin, on tumor endothelial cells (32, 33), which were negative for membrane Hsp70 (34).

Another recently discovered tumor targeting strategy involves the chemokine receptor CXCR4. Similar to Hsp70, CXCR4 offers the possibility to target different tumor entities.

However, some carcinomas, like the NSCLC, do not or only weakly express CXCR4 on their plasma membranes (35, 36). In contrast, Hsp70 is present on all tested NSCLC tumors (xenograft, primary human tumors; ref. 5). Furthermore, potential adverse effects of targeting CXCR4, such as the mobilization of hematopoietic progenitor cells by CXCR4 antagonists (37), remain to be elucidated.

The current study found no evidence that TPP has any toxic side effects, even if it was administered at 10-fold higher doses than those that were used for *in vivo* imaging. *Ex vivo* biodistribution analysis revealed the beneficial tumor-homing capacities of the TPP peptide. Although TPP was effectively washed out of the normal tissue 24 hours after its administration, pronounced levels remained within the tumor tissue at this time point (Fig. 2). The small-molecular weight of TPP ensures that it is cleared via the kidneys and does not accumulate in the liver like high-molecular weight targeting probes such as antibodies. As a consequence, TPP did not result in nonspecific background signals in the liver. Therefore, TPP could be used as an imaging probe for hepatocellular carcinoma and liver metastases (15).

In conclusion, TPP might be a useful peptide-based marker for diagnostic tumor targeting, as well as an efficient tool for drug delivery for a broad variety of human tumors.

#### **Disclosure of Potential Conflicts of Interest**

S. Stangl and G. Multhoff have ownership interest in a patent. V. Ntziachristos has ownership interest (including patents) in iThera Medical GmbH and is a consultant/advisory board member for iThera Medical GmbH. No potential conflicts of interest were disclosed by the other authors.

#### **Authors' Contributions**

Conception and design: S. Stangl, V. Ntziachristos, G. Multhoff

Development of methodology: S. Stangl

Acquisition of data (provided animals, acquired and managed patients, provided facilities, etc.): S. Stangl, J. Varga, B. Freysoldt, M. Trajkovic-Arsic, J.T. Siveke, G. Multhoff

Analysis and interpretation of data (e.g., statistical analysis, biostatistics, computational analysis): S. Stangl, J. Varga, B. Freysoldt, J.T. Siveke, V. Ntziachristos, G. Multhoff

Writing, review, and/or revision of the manuscript: S. Stangl, J. Varga, J.T. Siveke, V. Ntziachristos, G. Multhoff

Administrative, technical, or material support (i.e., reporting or organizing data, constructing databases): S. Stangl, V. Ntziachristos
Study supervision: F.R. Greten, G. Multhoff

#### **Grant Support**

This work was supported by the German Research Foundation (DFG) Collaborative Research Center SFB824/B4—"Imaging for Selection, Monitoring and Individualization of Cancer Therapies."

The costs of publication of this article were defrayed in part by the payment of page charges. This article must therefore be hereby marked *advertisement* in accordance with 18 U.S.C. Section 1734 solely to indicate this fact.

Received February 14, 2014; revised August 11, 2014; accepted August 27, 2014; published Online First October 9, 2014.

#### References

- Snyder EL, Dowdy SF. Cell penetrating peptides in drug delivery. Pharm Res 2004;21:389–93.
- Kondo E, Saito K, Tashiro Y, Kamide K, Uno S, Furuya T, et al. Tumour lineage-homing cell-penetrating peptides as anticancer molecular delivery systems. Nat Commun 2012;3:951.
- El-Andaloussi S, Holm T, Langel U. Cell-penetrating peptides: mechanisms and applications. Curr Pharm Des 2005;11: 3597-611.
- Farkas B, Hantschel M, Magyarlaki M, Becker B, Scherer K, Landthaler M, et al. Heat shock protein 70 membrane expression and melanoma-

- associated marker phenotype in primary and metastatic melanoma. Melanoma Res 2003:13:147–52.
- Hantschel M, Pfister K, Jordan A, Scholz R, Andreesen R, Schmitz G, et al. Hsp70 plasma membrane expression on primary tumor biopsy material and bone marrow of leukemic patients. Cell Stress Chaperones 2000:5:438–42.
- Sakamoto M, Effendi K, Masugi Y. Molecular diagnosis of multistage hepatocarcinogenesis. Japanese J Clin Oncol 2010;40:891–6.
- Sherman M, Multhoff G. Heat shock proteins in cancer. Ann N Y Acad Sci 2007;1113:192–201.
- Kurahashi T, Miyake H, Hara I, Fujisawa M. Expression of major heat shock proteins in prostate cancer: correlation with clinicopathological outcomes in patients undergoing radical prostatectomy. J Urol 2007;177:757–61.
- Multhoff G, Botzler C, Jennen L, Schmidt J, Ellwart J, Issels R. Heat shock protein 72 on tumor cells: a recognition structure for natural killer cells. J Immunol 1997;158:4341–50.
- Radons J, Multhoff G. Immunostimulatory functions of membranebound and exported heat shock protein 70. Exerc Immunol Rev 2005;11:17–33.
- Nylandsted J, Gyrd-Hansen M, Danielewicz A, Fehrenbacher N, Lademann U, Hoyer-Hansen M, et al. Heat shock protein 70 promotes cell survival by inhibiting lysosomal membrane permeabilization. J Exp Med 2004:200:425–35.
- Steiner K, Graf M, Hecht K, Reif S, Rossbacher L, Pfister K, et al. High HSP70-membrane expression on leukemic cells from patients with acute myeloid leukemia is associated with a worse prognosis. Leukemia 2006;20:2076–9.
- **13.** Thanner F, Sutterlin MW, Kapp M, Rieger L, Kristen P, Dietl J, et al. Heat-shock protein 70 as a prognostic marker in node-negative breast cancer. Anticancer Res 2003;23:1057–62.
- Pfister K, Radons J, Busch R, Tidball JG, Pfeifer M, Freitag L, et al. Patient survival by Hsp70 membrane phenotype: association with different routes of metastasis. Cancer 2007;110:926–35.
- Li H, Sui C, Kong F, Zhang H, Liu J, Dong M. Expression of HSP70 and JNK-related proteins in human liver cancer: potential effects on clinical outcome. Dig Liver Dis 2007;39:663–70.
- Stangl S, Gehrmann M, Dressel R, Alves F, Dullin C, Themelis G, et al. In vivo imaging of CT26 mouse tumours by using cmHsp70.1 monoclonal antibody. J Cell Mol Med 2011;15:874–87.
- Stangl S, Gehrmann M, Riegger J, Kuhs K, Riederer I, Sievert W, et al. Targeting membrane heat-shock protein 70 (Hsp70) on tumors by cmHsp70.1 antibody. Proc Natl Acad Sci U S A 2011;108:733–8.
- Gehrmann M, Foulds GA, Breuninger S, Stangl S, Pockley AG, Multhoff G. Tumor imaging and targeting potential of an Hsp70-derived 14-mer peptide. PLoS ONE 2014;28:9e105344.
- Mahalka AK, Kirkegaard T, Jukolal, Jäättelä M, Kinnunen PHJ. Human heat shock protein 70 (Hsp70) as a peripheral membrane protein. Biochim Biophys Acta 2014;1838:1344–61.
- Greten FR, Eckmann L, Greten TF, Park JM, Li ZW, Egan LJ, et al. IKKbeta links inflammation and tumorigenesis in a mouse model of colitis-associated cancer. Cell 2004;118:285–96.
- Ardito CM, Gruner BM, Takeuchi KK, Lubeseder-Martellato C, Teichmann N, Mazur PK, et al. EGF receptor is required for KRAS-induced pancreatic tumorigenesis. Can Cell 2012;22:304–17.

- Themelis G, Harlaar NJ, Kelder W, Bart J, Sarantopoulos A, van Dam GM, et al. Enhancing surgical vision by using real-time imaging of alphaVbeta3-integrin targeted near-infrared fluorescent agent. Ann Surg Oncol 2011;18:3506–13.
- 23. Hosotani R, Kawaguchi M, Masui T, Koshiba T, Ida J, Fujimoto K, et al. Expression of integrin alphaVbeta3 in pancreatic carcinoma: relation to MMP-2 activation and lymph node metastasis. Pancreas 2002;25: e30–5
- 24. Cardoso F, Saghatchian M, Thompson A, Rutgers ECommittee TCS. Inconsistent criteria used in American Society of Clinical Oncology 2007 update of recommendations for the use of tumor markers in breast cancer. J Clin Oncol 2008;26:2058–9.
- 25. McShane LM, Altman DG, Sauerbrei W, Taube SE, Gion M, Clark GM, et al. REporting recommendations for tumor MARKer prognostic studies (REMARK). Nat Clin Pract Oncol 2005;2:416–22.
- 26. Schilsky RL, Taube SE. Tumor markers as clinical cancer tests are we there yet? Semin Oncol 2002;29:211–2.
- 27. Barrott JJ, Hughes PF, Osda T, Yang XY, Hartman ZC, Loiselle DR, et al. Optical and radioiodinated tethered Hsp90 inhibitors reveal selective internalization of ectotpic Hsp90 in malignant breast tumor cells. Chem Biol 2013;20:1187–97.
- He T, Xue Z, Lu K, Valdivia Y, Alvarado M, Wong KK, et al. A minimally invasive multimodality image-guided (MIMG) system for peripheral lung cancer intervention and diagnosis. Comput Med Imaging Graph 2012;36:345–55
- 29. Valvidia Y, Alvarado M, Wong K, He TC, Xue Z, Wong ST. Image-guided fiberoptic molecular imaging in a VX2 rabbit lung tumor model. J Vasc Interv Radiol 2011;22:1758–64.
- Trajkovic-Arsic M, Mohajerani P, Sarantopoulos A, Kalideris E, Steiger K, Esposito I, et al. Multimodal molecular imaging of integrin avβ3 for *in vivo* detection of pancreatic cancer. J Nucl Med 2014; 55:446–51.
- Desgrosellier JS, Cheresh DA. Integrins in cancer: biological implications and therapeutic opportunities. Nat Rev Cancer 2010; 10:9–22.
- **32.** Brooks PC, Clark RA, Cheresh DA. Requirement of vascular integrin alphaVbeta3 for angiogenesis. Science 1994;264:569–71.
- 33. Ruegg C, Yilmaz A, Bieler G, Bamat J, Chaubert P, Lejeune FJ. Evidence for the involvement of endothelial cell integrin alphaVbeta3 in the disruption of the tumor vasculature induced by TNF and IFN-gamma. Nat Med 1998;4:408–14.
- 34. Gehrmann M, Stangl S, Kirschner A, Foulds GA, Sievert W, Doss BT, et al. Immunotherapeutic targeting of membrane Hsp70-expressing tumors using recombinant human granzyme B. PLoS ONE 2012;7: e41341.
- 35. Burger M, Glodek A, Hartmann T, Schmitt-Graff A, Silberstein LE, Fujii N, et al. Functional expression of CXCR4 (CD184) on small-cell lung cancer cells mediates migration, integrin activation, and adhesion to stromal cells. Oncogene 2003;22:8093–101.
- Burger JA, Kipps TJ. CXCR4: a key receptor in the crosstalk between tumor cells and their microenvironment. Blood 2006;107: 1761–67.
- Liles WC, Broxmeyer HE, Rodger E, Wood B, Hubel K, Cooper S, et al. Mobilization of hematopoietic progenitor cells in healthy volunteers by AMD3100, a CXCR4 antagonist. Blood 2003;102:2728–30.



## **Cancer Research**

The Journal of Cancer Research (1916–1930) | The American Journal of Cancer (1931–1940)

### Selective In Vivo Imaging of Syngeneic, Spontaneous, and Xenograft Tumors Using a Novel Tumor Cell-Specific Hsp70 **Peptide-Based Probe**

Stefan Stangl, Julia Varga, Bianca Freysoldt, et al.

Cancer Res 2014;74:6903-6912. Published OnlineFirst October 9, 2014.

**Updated version** Access the most recent version of this article at:

doi:10.1158/0008-5472.CAN-14-0413

Access the most recent supplemental material at: Supplementary

http://cancerres.aacrjournals.org/content/suppl/2014/10/08/0008-5472.CAN-14-0413.DC1.html Material

Cited articles This article cites 37 articles, 9 of which you can access for free at: http://cancerres.aacrjournals.org/content/74/23/6903.full.html#ref-list-1

Sign up to receive free email-alerts related to this article or journal. E-mail alerts

Reprints and pubs@aacr.org. Subscriptions

To order reprints of this article or to subscribe to the journal, contact the AACR Publications Department at

To request permission to re-use all or part of this article, contact the AACR Publications Department at **Permissions** 

permissions@aacr.org.